

# The Spectral Energy Distribution of Quiescent Black Hole X-ray Binaries: New Constraints from *Spitzer*

Elena Gallo<sup>1,2</sup>, Simone Migliari<sup>3</sup>, Sera Markoff<sup>4</sup>, John A. Tomsick<sup>5</sup>, Charles D. Bailyn<sup>6</sup>, Stefano Berta<sup>3,7</sup>, Rob Fender<sup>8</sup>, James C. A. Miller-Jones<sup>4</sup>

## ABSTRACT

Among the various issues that remain open in the field of accretion onto black hole X-ray binaries (BHBs) is the way the gas accretes at very low Eddington ratios, in the so-called quiescent regime. While there is general agreement that the X-rays are produced by a population of high-energy electrons near to the BH, the controversy comes about in modeling the contribution from inflowing vs. outflowing particles, and their relative energy budget. Recent *Spitzer* observations of three quiescent BHBs have shown evidence for excess emission with respect to the Rayleigh-Jeans tail of the companion star between 8–24  $\mu\text{m}$ . We suggest that synchrotron emission from a partially self-absorbed outflow might be responsible for the observed mid-IR excess, in place of, or in addition to, thermal emission from circumbinary material. If so, then the jet synchrotron luminosity, integrated from radio up to near-IR frequencies, exceeds the measured 2–10 keV luminosity by a factor of a few in these systems. In turn, the mechanical power stored in the jet exceeds the bolometric X-ray luminosity at least by 4 orders of magnitude. We then compile the broadband spectral energy distribution (SED) of A0620–00, the lowest Eddington-ratio stellar mass BH with a known radio counterpart, by means of simultaneous radio, optical and X-ray observations,

---

<sup>1</sup>Physics Department, Broida Hall, University of California Santa Barbara, CA 93106

<sup>2</sup>Chandra Fellow

<sup>3</sup>Center for Astrophysics and Space Sciences, 9500 Gilman Dr., University of California San Diego, La Jolla, CA 92093

<sup>4</sup>Astronomical Institute ‘Anton Pannekoek’, University of Amsterdam, Kruislaan 403, 1098 SJ, Amsterdam, NL

<sup>5</sup>Space Sciences Laboratory, 7 Gauss Way, University of California Berkeley, CA 94720

<sup>6</sup>Department of Astronomy, Yale University, P.O. Box 208101, New Haven, CT 06520

<sup>7</sup>Dipartimento di Astronomia, Università di Padova, Vicolo dell’ Osservatorio 2, 35122 Padova, IT

<sup>8</sup>School of Physics and Astronomy, University of Southampton, Southampton SO17 1BJ, UK

and the archival *Spitzer* data. We are able to fit the SED of A0620–00 with a ‘maximally jet-dominated’ model in which the radio through the soft X-rays are dominated by synchrotron emission, while the hard X-rays are dominated by inverse Compton at the jet base. The fitted parameters land in a range of values that is reminiscent of the Galactic Center super-massive black hole Sgr A\*. Most notably, the inferred ratio of the jet acceleration rate to local cooling rates is two orders of magnitude weaker with respect to higher luminosity, hard state sources.

*Subject headings:* X-rays: binaries — radiation mechanisms: general — stars: individual (A0620–00, V404 Cyg, XTE J1118+480)

## 1. Introduction

The *Spitzer Space Telescope* offers the opportunity for the first time to identify and characterize the properties of highly sub-Eddington Galactic black hole X-ray binaries (BHBs) in the mid-infrared band, a frequency window that is still largely unexplored for these systems, and that can prove to be crucial for our understanding of the overall structure of the accretion flow in quiescence. The infrared (IR) spectra of BHBs with a low mass donor star are likely shaped by a number of competing emission mechanisms, among which: reprocessing of accretion-powered X-ray and ultraviolet photons, either by the donor star surface or by the outer accretion disk, direct thermal emission from the outer disk, non-thermal synchrotron emission from a relativistic outflow and thermal emission from circumbinary dust. We refer the reader to Russell et al. (2006; R06 hereafter), and references therein, for a recent comprehensive work on the optical and near-IR spectral properties of X-ray binaries. Here we wish to stress that, as well as for other wavebands, the relative strength of each mechanism is known to vary greatly in response to changes in the ‘X-ray state’ of the system (see McClintock & Remillard 2006; Homan & Belloni 2005). Throughout this work, we shall focus on the IR properties of hard and quiescent low mass BHBs. Such (generally transient) systems are characterized by strong variability, power-law dominated X-ray spectra, and integrated X-ray luminosities that are largely sub-Eddington (roughly between a few  $10^{-6} - 10^{-2}$  times the Eddington luminosity,  $L_{\text{Edd}}$ , for the hard state, and below a few  $10^{-6}L_{\text{Edd}}$  for the quiescent state).

In spite of the large degree of uncertainty on the overall geometry of the accretion flow in this regime, there is general agreement that the X-rays are produced by a population of high-energy electrons near to the BH, and that the accreting gas is highly inefficient at radiating, either as a result of an intrinsically reduced radiative efficiency (Narayan & Yi 1994), or because of a substantial mass loss (Blandford & Begelman 1999), or a combination of the two

(e.g. Markoff et al. 2001; Yuan et al. 2005). The hard state is associated with the production of persistent, partially self-absorbed, synchrotron-emitting outflows with flat/inverted radio-mm spectra (Fender 2001). Such jets appear to survive down to quiescent X-ray luminosities (Gallo et al. 2006), even though sensitivity limitations on current radio telescopes make it extremely difficult to reach the signal-to-noise ratios required to assess their presence for low luminosity systems farther than 2 kpc or so. There is evidence from large-scale structures that the jets’ mechanical power is comparable to the bolometric X-ray luminosity in some hard state sources (e.g. Cyg X-1, Gallo et al. 2005a; Russell et al. 2007). However, even for the highest quality spectral energy distribution (SED), disentangling the relative contributions of inflow vs. outflow to the radiation spectrum and global accretion energy budget can be quite challenging, as illustrated by the emblematic case of XTE J1118+480 in McClintock et al. (2003) and Markoff et al. (2001). Estimates of the total jet power based on its radiation spectrum depend crucially on the assumed frequency at which the flat, partially self-absorbed spectrum turns and becomes optically thin, as the jet ‘radiative efficiency’ depends ultimately on the location of the high-energy cutoff induced by the higher synchrotron cooling rate of the most energetic particles. Once again, this quantity has proved hard to measure.

R06 have collected all the available quasi-simultaneous optical and near-IR data of a large sample of Galactic X-ray binaries over different X-ray states. The optical/near-IR luminosity of hard/quiescent BHBs correlates with the X-ray luminosity to the power  $\sim 0.6$ , consistent with the known radio/X-ray correlation slope down to  $10^{-8}L_{\text{Edd}}$  (Gallo et al. 2006; but see Gallo 2007 and Xue & Cui 2007). Combined with the fact that the near-IR emission is largely suppressed in the thermal-dominant state (R06, Figure 4), this leads to the conclusion that, for the BHBs, the break to the optically thin portion would take place in the mid-IR (2-40  $\mu\text{m}$ ). Additional evidence for a synchrotron contribution to the IR band in hard state BHBs comes from variability studies during outbursts (e.g. Hynes et al. 2006; Homan et al. 2005). Indeed, from a theoretical point of view, the *break frequency*, here defined as the frequency at which the partially self-absorbed jet becomes optically thin, is inversely proportional to the BH mass: as jet spectral breaks are often observed in the GHz/sub-mm regime in active nuclei, they are expected to occur in the IR-optical band for  $10^{5-7}$  times lighter objects (see discussion in e.g. Markoff et al. 2001 and references therein). We know however from observations of GX 339–4, the only BHB where the optically thin jet spectrum has been perhaps observed (Corbel & Fender 2002; Homan et al. 2005), that the exact break frequency can vary with the overall luminosity, possibly reflecting changes in the magnetic field energy density, particle density and mass loading at the jet base (Nowak et al. 2005). Determining the location of the jet break as a function of the bolometric luminosity is important to assess the synchrotron contribution to the hard X-ray band, and may even highlight substantial differences among different classes of objects. As an example, the fact

that the optically thin jet IR-emission in GX 339–4 connects smoothly with the hard X-ray power law has led to challenge the ‘standard’ Comptonization scenario for the hard X-ray state of BHBs (Markoff et al. 2001). On the contrary, recent *Spitzer* observations of the ultra-compact *neutron star* X-ray binary 4U 0614+091 (while in a hard state) revealed that the break frequency must take place in the far-IR in this system, effectively ruling out a synchrotron origin for the X-ray power law (Migliari et al. 2006).

In addition to the jet, *Spitzer* observations of quiescent BHBs should be sensitive to possible emission from circumbinary material. Circumbinary disks may be formed as a result of mass outflow from the accretion disk, and have been invoked as an efficient process for the removal of orbital angular momentum in addition to gravitational radiation loss and/or magnetic braking (see Taam & Spruit 2001 in the context of cataclysmic variables). Alternatively, circumbinary material could be due to the presence of a post-supernova explosion fall-back disk, as argued in the case of the anomalous X-ray pulsar 4U 0142+61 (Wang et al. 2006). Munro & Mauerhan (2006; MM06 hereafter) report on *Spitzer* observations of four nearby low mass X-ray binaries: three BHBs plus one neutron star system. Excess mid-IR emission – with respect to the Rayleigh-Jeans tail of the donor blackbody spectrum – is detected from two (possibly all three) BH systems; MM06 attribute this bump to circumbinary dust that is illuminated by the low mass companion star. This would imply that the optically thick-to-thin jet break occurs in the mm regime, at much lower frequencies than, e.g., inferred by R06.

In this paper, we aim to reassess the relative contribution of the various emission components to the radio/IR/optical spectra of the BHBs A0620–00, V404 Cyg and XTE J1118+480 while in the quiescent state. We first report on the re-analysis of *Spitzer* observations, focusing on the rms estimate in the 24  $\mu\text{m}$  datasets (Section 2), then proceed by examining the SED of each source (Section 3). The origin of the detected mid-IR excess emission is discussed in Section 4. We finally focus on the broadband SED of A0620–00, a highly sub-Eddington ( $L_X/L_{\text{Edd}} \simeq 10^{-8}$ ) BHB for which we put together previously published radio/X-ray data, the *Spitzer* data and new optical data, all taken in 2005. We discuss the results of fitting the whole SED by means of a maximally jet-dominated model in Section 5. A summary is given in Section 6.

## 2. *Spitzer* observations

The BHBs A0620–00, V404 Cyg and XTE J1118+480 were observed by *Spitzer* between 2004 October and 2005 May as part of a survey of nearby low-mass X-ray binaries (PI: Munro, Program 3289). Photometry of the three targets was acquired using the Multi-band Imaging

Photometer for *Spitzer* (MIPS; Rieke et al. 2004) at  $24\ \mu\text{m}$  and the Infrared Array Camera (IRAC; Fazio et al. 2004) at  $8$  and  $4.5\ \mu\text{m}$ . The Basic Calibrated Data (BCD) were re-processed and then mosaicked with the Mopex software (Makovoz & Marleau 2005), which uses single, multi-frame, and dual outlier rejection. As discussed by MM06, in the case of A0620–00, the MIPS image was affected by dark latent features from a previous observation. The artifacts were corrected by dividing each BCD frame by a normalized median frame (based on all BCDs excluding the source). These corrected BCDs were then mosaicked using Mopex. Unique IR counter-parts, consistent with the radio positions, are significantly ( $> 5\sigma$ ) detected at  $4.5$  and  $8\ \mu\text{m}$  for all the three sources. The MIPS  $24\ \mu\text{m}$  images of the targets are shown in Figure 1: V404 Cyg and A0620–00 are detected at the  $2$ - $2.5\sigma$  level, while XTE J1118+480 is undetected.

For each counterpart, we constructed the observation-specific point-response function (PRF) with `Prf_estimate`, and extracted the source flux using both standard aperture photometry on the background-subtracted image and PRF-fitting (using `Apex`), taking care to mask foreground stars. Sky subtraction was carried out through the use of multiple  $10$  arcsec sky apertures placed over an annulus around the source. Table 1 lists the fluxes as measured using both aperture photometry and PRF-fitting on the mosaic images (the measured fluxes were then corrected for interstellar extinction following the standard prescription for the frequency-variable absorption by Cardelli et al. 1989). The values obtained with the two methods are consistent with each other within the errors. While they are also consistent, within the errors, with those measured by MM06, we derive systematically larger (typically by a factor 3) rms noise levels for the MIPS  $24\ \mu\text{m}$  fluxes. In fact, statistical uncertainties related to sky subtraction are usually negligible compared to calibration and systematic uncertainties. However, statistical uncertainties can be appreciable – tens of percent – for low signal/noise sources (e.g. Dale et al. 2005). At  $24\ \mu\text{m}$ , this is clearly the case for A0620–00 and V404 Cyg, which are both affected by high cirrus background, as apparent from Figure 1.

### 3. Radio/Infrared/Optical spectra

We first compile the SEDs of the three systems by putting together the *Spitzer* data discussed above, plus optical and radio data available in the literature. For A0620–00, we make use of new optical data, presented in Section 3.3.1. Clearly, the non-strict simultaneity of the observations, combined with the known variability of quiescent BHBs at all wavelengths (e.g. Hynes et al. 2003, 2004), should be kept in mind before drawing any definitive conclusion on the modeling. Figure 2 shows the broadband SEDs of V404 Cyg, XTE J1118+480 and A0620–00, while in the quiescent state, from radio to optical wavelengths.

We first focus on the IR-optical spectra: unlike MM06, we do not compare the data against stellar atmosphere models: the smoothness of our SEDs does not demand a sophisticated model which can account for fine spectral features. Most importantly, we aim to quantify the relative goodness of the various models via proper  $\chi^2$  fitting, which would be meaningless if we were to apply stellar atmosphere codes to our sparse data-points. Hence, for each object we first model the IR-optical spectrum with a single temperature blackbody, using the best available estimates for the source distance, inclination and effective temperature. The blackbody approximation is meant to mimic the contribution from the donor star. As shown by MM06, the contribution from the irradiated outer accretion disk is negligible for the parameter space relevant to these quiescent systems, at least in the IR band. The best-fitting blackbody curves are shown in the left panels of Figure 3, with the fitted parameters and reduced  $\chi^2$  given in Table 2. Evidently, the single blackbody model provides a poor fit to the data: excess mid-IR emission, with respect to the Rayleigh-Jeans tail of the donor/disk, is detected in all three cases.

Fitting the data with two blackbodies (Figure 3, middle panels) slightly improves the reduced  $\chi^2$  in all cases (Table 3). The temperatures and normalizations of these secondary blackbodies imply indeed larger physical sizes than the orbital separation, possibly supporting the circumbinary material interpretation (MM06). However, radio emission has been detected in two of these sources (V404 Cyg: Hjellming et al. 2000, and A0620–00, Gallo et al. 2006), and interpreted as partially self-absorbed synchrotron emission from a relativistic outflow. The flat/slightly inverted outflow spectrum must become optically thin at higher frequencies, possibly in the mid-IR (R06). We thus explore the possibility that the mid-IR excess might be, at least partly, due to non-thermal emission from a jet. This possibility has been ruled out by MM06 on the basis of far too low fluxes/upper limits at  $24 \mu\text{m}$ . However, our revised estimates for the  $24 \mu\text{m}$  rms noise levels leave this possibility open.

We choose to fit the *radio*/IR/optical SEDs with a single blackbody plus a broken power law of the form:

$$F_\nu = F_{\nu_0} \times \begin{cases} (\nu/\nu_0)^{\alpha_1}, & \nu < \nu_b \\ (\nu_b/\nu_0)^{(\alpha_1-\alpha_2)}(\nu/\nu_0)^{\alpha_2}, & \nu > \nu_b \end{cases} \quad (1)$$

This is meant to account for a partially self-absorbed synchrotron spectrum with index  $\alpha_1 = 0.0 - 0.5$  up to the break frequency  $\nu_b$ , above which it becomes optically thin with index  $\alpha_2$ . After running a grid of models with all the six fitting parameters (blackbody temperature and normalization, plus the four broken power law parameters) free to vary, we choose to fix the index of the optically thin portion to  $\alpha_2 = -0.8$  (corresponding to a ‘canonical’ electron distribution  $N(E) \propto E^{-p}$  with power law index  $p = +2.6$ ,  $E$  being the electron energy; e.g. Fender 2006) and the position of the break to  $\nu_b = 10^{14}$  Hz, in order to maximize the jet contribution to the mid-IR band. The results of the blackbody plus

broken power law fits are shown in the right panels of Figure 3, with the fitted parameters in Table 4. We discuss below the SED compilation and the results of the modeling on a case by case basis.

### 3.1. V404 Cyg (GS 2023+338)

Casares et al. (1993) report on *B-V-R-J-H-K* band photometry of V404 Cyg taken in 1991 July-August, 2 years after the end of the 1989 outburst that preceded the current quiescent regime (even though this system, because of its relatively high quiescent X-ray luminosity [ $L_X/L_{\text{Edd}} \simeq 10^{-6.5}$ ], is often considered at the boundary between ‘quiescence’ and the hard X-ray state). Several later works have established V404 Cyg to be variable by a factor of a few at IR-to-X-ray wavelengths (see e.g. Hynes et al. 2004, Bradley et al. 2007 for the X-ray/optical variability; Zurita et al. 2004 for a study of the long term optical/IR variability, and references therein). The origin of such variability is yet to be well understood, even though there is general agreement that it should take place somewhere in the accretion flow rather than in the hot gas stream/donor star (Shahbaz et al. 2003; Zurita et al. 2003; Hynes et al. 2003; 2004).

Over the past few years, V404 Cyg has been known as a relatively stable radio source, with an average flux density of  $\sim 350 \mu\text{Jy}$ , and a flat/slightly inverted spectrum at GHz frequencies (Hjellming et al. 2000; Gallo et al. 2005b), interpreted in terms of partially self-absorbed synchrotron radiation from outflowing plasma. The variable nature of this system, combined with the fact that the available data spread an interval of several years (the optical and *Spitzer* data were acquired more than 10 years apart), make it especially difficult to draw definite conclusions about the mid-IR emission detected with MIPS (on the other hand, R06 showed that the optical-IR luminosity of hard/quiescent state sources scales with the X-ray luminosity to the power 0.6, implying that the X-ray variability should be reduced to some extent in the IR).

The top panels of Figure 3 show the IR-optical spectrum of V404 Cyg as fitted with a single and double blackbody model (left and middle panel, respectively): clearly the latter model provides a better fit to the IR-optical data, with  $\chi^2/\text{d.o.f.}=10.3/7$  and  $\chi^2/\text{d.o.f.}=1.4/5$ , respectively. However, these components do not account for the radio emission. Because of the flat radio spectrum, it can not be ruled out that the excess emission at  $24 \mu\text{m}$  might be due to the high frequency portion of the well-established synchrotron-emitting outflow. The top right panel of Figure 3 shows a fit to the radio-IR-optical data with a single blackbody with  $T \simeq 4600 \text{ K}$  plus a broken power law, where the fitted index of the partially self-absorbed regime is  $\alpha_1 = 0.02$ . This two-component model provides as a good fit as the

double blackbody model ( $\chi^2/\text{d.o.f.}=4.0/9$ ), and it also accounts for the radio emission.

This suggests that, in this system, synchrotron emission from a partially self-absorbed outflow is likely to be responsible for the observed mid-IR excess as much as thermal emission from circumbinary material. As an aside, if such excess were entirely due to circumbinary disk emission, this would imply that the jet break to the optically thin portion has to occur somewhere in the mm regime, i.e. at lower frequencies than predicted by R06. While the system SED could be comfortably reproduced by the sum of two blackbody components plus a broken power law, accommodating the circumbinary material and jet the contribution, this would require as many free parameters as data points.

### 3.2. XTE J1118+480

Gelino et al. (2006) present  $B-V-R-J-H-K_S$  band photometry of XTE J1118+480 in quiescence. Due to its high Galactic latitude, XTE J1118+480 is a virtually unabsorbed source ( $A_V = 0.06$ ) and yet it can be taken as an example of how tricky it can be to infer the properties and the geometry of the accretion flow based on modeling the SED. For instance, the high quality simultaneous multi-wavelength data acquired while in the hard state (at  $L_X/L_{\text{Edd}} \simeq 10^{-3}$ ) have been successfully modeled in terms of an advection-dominated accretion flow (McClintock et al. 2003; Yuan et al. 2005), as well as using a jet synchrotron model (Markoff et al. 2001). As shown in Figure 3, middle panels, there is evidence for substantial excess emission at  $8 \mu\text{m}$  with respect to the donor star tail. We notice that the single blackbody model provides a very poor representation of the donor star spectrum: in this case, the actual stellar atmosphere model is certainly more appropriate (see MM06, Figure 2). However, as noticed above, we are interested in constraining the nature of the excess mid-IR emission via proper  $\chi^2$  fitting: in this framework, irrespective of how well the donor star thermal emission is modeled, our goal is to determine whether fitting the mid-IR excess with a broken power law model provides a better or worse description of the data in a statistical sense. The radio counterpart to XTE J1118+480 is undetected in quiescence, with an upper limit of 0.1 mJy at 8.5 GHz (Mirabel et al. 2001). Because of this shallow upper limit, the measured excess at  $8 \mu\text{m}$  might still be interpreted as due to a partially self-absorbed outflow that extends its power-law spectrum from the radio up to the IRAC regime. This is illustrated in middle right panel of Figure 3, where a partially self-absorbed synchrotron emitting outflow with  $\alpha_1 = 0.27$ , plus a  $\sim 4300$  K blackbody component, account for the system SED. The reduced  $\chi^2$  is improved with respect to the double blackbody model ( $\chi^2/\text{d.o.f.} = 12.0/3$  vs.  $6.2/3$ , respectively for the double blackbody and blackbody plus broken power law model). Within the blackbody plus power-law model,



the fitted values for the blackbody temperature and normalization are consistent, within the errors, with the inferred values for the donor star (namely  $\sim 4250$  K and  $\simeq 0.4 R_{\odot}$ ; Gelino et al. 2006). The fitted radio spectral index is consistent with hard state sources (Fender 2001), and predicts a GHz flux density lower than  $5 \mu\text{Jy}$ , practically undetectable with current radio facilities over reasonable integration times (the rms noise level for a 24 hr integration with the VLA is about  $5 \mu\text{Jy}$  at 8.5 GHz; however, planned upgrades, such as the eMERLIN and EVLA will be able to probe such flux density levels in hrs-long exposures).

### 3.3. A0620–00 (V616 Mon)

#### 3.3.1. SMARTS observations

We construct the SED of A0620–00 by means of radio, IR, optical and X-ray observations, all taken in 2005; the optical/near-IR data were acquired by the Small and Moderate Aperture Research Telescope System (SMARTS<sup>1</sup>) consortium, using the Cerro Tololo Inter-American Observatory (CTIO) 1.3 m together with ANDICAM<sup>2</sup>, a dual-channel imager capable of obtaining optical and IR data simultaneously. A0620–00 was observed through *I-V-H* filters on 2005 August 18, one day before the beginning of the (strictly simultaneous) Chandra/VLA observations (taken on 2005 August 19-20; Gallo et al. 2006), while the *Spitzer* data discussed above were acquired on 2005 March 06 (MIPS) and March 25 (IRAC).

SMARTS data were calibrated using data from previous nights and were processed and reduced using standard IRAF aperture photometry routines. The measured magnitudes were converted into fluxes using the SMARTS photometric zero-points; we used a color excess of  $E(B - V) = 0.39 \pm 0.02$  (Wu et al. 1976), and corrected for extinction following again the standard prescription for the frequency-variable absorption by Cardelli et al. (1989). The results are summarized in Table 5. Interestingly, all of the measured magnitudes are brighter than the maximum magnitude from the previously published quiescent light-curves (see Table 1 in Gelino et al. 2001, reporting on optical and IR observations of A0620–00 between 1976 and 2001), and from 0.5-0.7 mag brighter than the mean magnitudes. However, given the observed trend over the past few years of increasing brightness in this source, it seems very unlikely that these results require a sudden flare. This however has to be kept in mind when inspecting the whole SED of A0620–00, in particular when comparing the 2005 March *Spitzer* observations with the optical, near-IR values given by Gelino et al. (2001).

---

<sup>1</sup><http://www.astro.yale.edu/smarts>

<sup>2</sup><http://www.astronomy.ohio-state.edu/ANDICAM>

### 3.3.2. Broadband SED

Significant excess emission with respect to the Rayleigh-Jeans portion of the donor’s blackbody spectrum is detected at 8 and 24  $\mu\text{m}$ . As shown in the middle-bottom panel of Figure 3, the sum of two blackbodies ( $\sim 4700 + 390$  K) provides a good fit to the IR-optical data ( $\chi^2/\text{d.o.f.}=2.0/2$ ). The detection of a radio counterpart to A0620–00 strongly suggests that this quiescent system is powering a synchrotron-emitting outflow (Gallo et al. 2006). Arbitrarily assuming a flat spectrum for the partially self-absorbed portion of the jet, this would have to become optically thin at frequencies lower than  $10^{13}$  Hz for it not to contribute to the mid-IR excess. Alternatively, the whole radio-IR-optical spectrum can be well fit by the sum of  $\sim 4900$  K blackbody plus a broken power law with slightly inverted spectrum in the radio-IR regime with  $\alpha_1 = 0.1$  (yielding  $\chi^2/\text{d.o.f.}=7.8/3$ ).

## 4. Origin of the mid-IR excess: implications for the jet power

The *Spitzer* observations of three quiescent BHBs discussed above show evidence for excess emission in the mid-IR band; while it may possible to reproduce the emission between  $2-4 \times 10^{14}$  Hz with a blackbody whose temperature is consistent with the shown temperatures of the secondary stars, it would be difficult to explain the excess at  $10^{13}$  Hz with any model for which the temperature is high enough so that  $10^{13}$  Hz is in the Rayleigh-Jeans portion of the blackbody spectrum. Thus, two main possibilities arise to account for the measured excess: thermal emission from cool (hundreds of K) circumbinary material, or synchrotron emission from outflowing plasma. The latter hypothesis was dismissed by MM06 on the basis of far too low 24  $\mu\text{m}$  fluxes/upper limits. Our estimates for the statistical uncertainties on the 24  $\mu\text{m}$  observations, however, reinstate this possibility.

Under the assumption that non-thermal synchrotron emission is at the origin of the measured IR-excess, we can estimate the amount of power stored in the outflows. Integrating the partially self-absorbed jet spectra up to  $10^{14}$  Hz, and assuming a (conservatively low) jet radiative efficiency of 5%, and no Doppler boosting (see Fender 2001), we obtain jet powers in the range  $\sim 4 \times 10^{32}$  erg  $\text{s}^{-1}$ , for A0620–00 and XTE J1118+480, the lower Eddington ratio sources, up to  $\sim 2 \times 10^{34}$  erg  $\text{s}^{-1}$ , for V404 Cyg (see Table 6). Under these assumptions, the total jet power exceed the measured X-ray luminosities (between 2-10 keV) in quiescence by a factor 50 at least. Assuming that the steep X-ray power laws observed in quiescent BHBs (with average photon index  $\Gamma \simeq 2$ ; e.g. Corbel et al. 2006) extend up to  $\sim 100$  keV, where a spectral cutoff is observable in higher Eddington-ratio systems, the *bolometric* (0.1-100 keV) X-ray luminosities are likely to exceed the measured 2-10 keV luminosities by a factor of a few. Therefore, this regime of  $L_{\text{j,tot}} \gtrsim L_{\text{X}}$  fits the definition of

‘jet-dominated’ state put forward by Fender et al. (2003). The above estimates of  $L_{j,\text{tot}}$  are based on a conservative radiative efficiency for the synchrotron process of 5%; as such, they represent strict lower limits. Alternatively, we can estimate the total jet power following the formalism by Heinz & Grimm (2005), where the monochromatic radio core emission ( $L_r$ , in units of  $10^{30}$  erg s $^{-1}$ ) of three well studied radio galaxies was directly compared to the radio lobe emission, and combined with a self-similar jet model (Heinz & Sunyaev 2001) in order to calibrate the ratio of mechanical vs. radiative power of partially self-absorbed jets. They proposed that the jet kinetic power of both super-massive and stellar size BHs can be estimated from the core radio luminosity as:  $L_{j,\text{tot}} = 6.2 \times 10^{37} L_r^{1/(1.4-\alpha_r/3)} \mathcal{W}_{37.8}$  erg s $^{-1}$ , where  $\alpha_r$  is the radio spectral index over the partially self-absorbed regime, and the parameter  $\mathcal{W}_{37.8}$  carries the (quite large) uncertainty on the radio galaxy calibration. The normalization value by Heinz & Grimm is roughly in agreement to that estimated by K rding et al. (2006): here, for flat spectrum radio sources, the jet power (at the hard to soft state transition) is expressed as:  $L_{j,\text{tot}} \lesssim 3.6 \times 10^{37} (f/0.75)(\eta/0.1) L_r^{(12/17)}$  erg s $^{-1}$ ,  $f$  being the fraction of outer mass accretion rate that is not expelled via winds/outflows, and  $\eta$  the standard accretion efficiency. Either way, the inferred total jet power would exceed the *bolometric* X-ray luminosity by at least 4 orders of magnitude for the three quiescent BHBs under consideration. It is worth mentioning that, independently of normalization and efficiency factors, in all three cases the jet *synchrotron* luminosity, integrated up to  $10^{14}$  Hz (that is neglecting the optically thin portion), already exceed the measured 2-10 keV luminosities by a factor of a few (Table 6, right column).

In contrast, if thermal emission from circumbinary disk material is entirely responsible for the measured mid-IR excess, this would imply that the jet spectrum breaks at much lower frequencies, perhaps in far-IR/mm regime, lowering the above estimates by a factor of ten at least. A final test to assess the origin of the measured excess could be variability study in the mid-IR, possibly coordinated with the radio.

## 5. A maximally jet-dominated model for the quiescent state

Ultimately, as discussed by McClintock et al. (2003), while there is general agreement that the X-ray emission in quiescent BHBs comes from high-energy electrons near the BH, the disagreement comes about in: *i*) attributing the emission to outflowing vs. inflowing electrons; *ii*) modeling the electron distribution as thermal vs. non-thermal (or hybrid). The SEDs of quiescent BHBs, as well as low-luminosity AGN are often examined in the context of the advection-dominated accretion flow model (ADAF; Narayan & Yi 1994), whereby the low X-ray luminosities would be due to a highly reduced radiative efficiency, and most of the

liberated accretion power disappears into the horizon. Alternatively, building on the work by Falcke & Biermann (1995) on AGN jets, a jet model has been proposed for hard state BHBs. The model is based upon four assumptions: 1) the total power in the jets scales with the total accretion power at the innermost part of the accretion disk,  $\dot{m}c^2$ , 2) the jets are freely expanding and only weakly accelerated via their own internal pressure gradients only, 3) the jets contain cold protons which carry most of the kinetic energy while leptons dominate the radiation and 4) some fraction of the initially quasi-thermal particles are accelerated into power-law tails. Markoff et al. (2001) argued that jet synchrotron emission could account for the broad continuum features of the simultaneous radio through X-ray observations of XTE J1118+480 while in the hard state. This same model could also explain the broad spectral features of 13 quasi-simultaneous radio/X-ray observations of GX 339–4, and was able to reproduce the observed non-linear radio/X-ray correlation in this system (Corbel et al. 2003) by varying the amount of power that is channeled in the jet (Markoff et al. 2003). Based on the required reflection signatures a new model was developed (Markoff et al. 2005; MNW05 hereafter) which could reproduce the simultaneous radio/X-ray data of hard state systems (GX 339–4 and Cygnus X-1) via radiation from a compact, mildly relativistic jet, combined with a truncated thermal disk. In particular, the X-ray emission can be interpreted as a combination of optically thin synchrotron emission predominantly from an acceleration region  $\sim 10 - 100$  gravitational radii along the jets, plus external (thermal disk photons) and synchrotron self-Compton emission from the base of the jets, in a region associated with a magnetic compact corona. The radio through the soft X-rays are dominated by synchrotron emission, while the hard X-rays are mostly Comptonization, with weak reflection. This ‘*maximally jet-dominated model*’ was intended to explore the possibility that the ‘hot electron corona’ and ‘jet base’ may be intimately related, or, in the extreme case, synonymous (we refer the reader to MNW05 for a fuller description). This model has been tested extensively on simultaneous radio and X-ray data, and for a number of hard state BHBs. The mid-IR portion of the spectrum is clearly crucial in order to put constraints on the optically thick-to-thin jet breaks, as demonstrated by the *Spitzer* observations of the neutron star X-ray binary 4U 0614+091 (Migliari et al. 2006) and the BHB GRO 1655–40 (Migliari et al. , submitted to ApJ).

In the following we attempt to fit the radio through X-rays SED of A0620–00 in quiescence via the maximally jet-dominated model, where full details can be found in the Appendix of MNW05. The choice of A0620–00 (over e.g. V404 Cyg, for which the radio spectrum is well constrained) is motivated by the fact that, with the exception of the *Spitzer* data, the observations were acquired nearly-simultaneously (the VLA/*Chandra* observations were strictly simultaneous, while the SMARTS observations were taken only one day apart). As a comparison, the broadband SED of V404 Cyg is built on datasets that were

taken over 10 years apart. In addition, A0620–00 has been in quiescence for over 30 years, and is considered as a stable and moderately variable system, while V404 Cyg is known to vary in flux by a factor of a few within hours (e.g. Hynes et al. 2003).

### 5.1. Application to A0620–00

The fitting was performed with the INTERACTIVE SPECTRAL INTERPRETATION SYSTEM (ISIS; Houck & De Nicola 2000). As outlined in MNW05, the fitting is initiated outside ISIS in order to avoid local minima, using unfolded data that yield a set of starting parameters for which the reduced  $\chi^2$  is lower than 2. We have decided to fix several parameters which previously have been allowed to vary, in some cases because the results of fitting the model to several hard state sources suggest that there may be canonical values, and secondly because of the low count rates. In spite of the large luminosity difference between A0620–00 ( $L_X/L_{\text{Edd}} \simeq 10^{-8}$ ) and other sources whose hard state spectra were successfully fitted by the jet model, such as XTE J1118+480 (Markoff et al. 2001), GX339–4 and Cygnus X–1 (Markoff et al. 2005), simultaneous VLA/*Chandra* observations of A0620–00 in quiescence have shown that the non-linear radio/X-ray correlation for hard state BHBs appears unbroken all the way down to  $10^{-8}L_{\text{Edd}}$ , arguing for no substantial difference between hard and quiescent state (Gallo et al. 2006; but see Xue & Cui 2007 and Gallo 2007). On the other hand, recent high statistics X-ray observations of hard state BHBs seem to show that a geometrically thin disk is present and extends close to the innermost stable orbit already at  $10^{-3}L_{\text{Edd}}$  (Miller et al. 2006a, 2006b; Rykoff et al. 2007). As such solution would be very difficult to maintain at  $10^{-8}L_{\text{Edd}}$ , these authors conclude that a major transition has to take place at intermediate luminosities. Consequently, in light of the large degree of uncertainty over the nature and geometry of the accretion flow in quiescence, this must be considered as an exploratory study.

The model is most sensitive to the fitted parameter  $N_j$ , which acts as a normalization, though it is not strictly equivalent to the total power in the jets (see discussion in MNW05). It dictates the power initially divided between the particles and magnetic field at the base of the jet, and is expressed in terms of a fraction of  $L_{\text{Edd}}$ . Once  $N_j$  is specified and conservation is assumed, the macroscopic physical parameters along the jet are determined assuming that the jet power is roughly shared between the internal and external pressures. The radiating particles enter the base of the jet where the bulk velocities are lowest, with a quasi-thermal distribution. Starting at location  $z_{\text{acc}}$  in the jets, a free parameter, a fraction 85% of the particles are accelerated into a powerlaw with index  $p$ , also a fitted parameter. The maximum energy of the accelerated leptons is calculated by setting the acceleration rate to the local

cooling rates from synchrotron and inverse Compton radiation at  $z_{\text{acc}}$ . If the acceleration process is diffusive Fermi acceleration, the acceleration rate depends on the factor  $f = \frac{(u_{\text{acc}}/c)^2}{f_{\text{sc}}}$ , where  $u_{\text{acc}}$  is the shock speed relative to the bulk plasma flow, and  $f_{\text{sc}}$  is the ratio of the scattering mean free path to the gyro-radius. Because neither plasma parameter is known, we fit for their combined contribution via  $f$ , which thus reflects the *efficiency of acceleration*. The particles in the jet radiatively cool via adiabatic expansion, the synchrotron process, and inverse Compton up-scattering; however, adiabatic expansion is assumed to dominate the observed effects of cooling. A weak thermal accretion disk is assumed to be present, with an inner disk temperature (somewhat arbitrarily) fixed at  $T = 10^6$  K, or  $\sim 90$  eV (inner disk temperatures between 50–200 keV are typically obtained for higher Eddington ratio sources). This component is also included in the Figure 4 and its photons are considered for local inverse Compton up-scattering. However they are negligible compared to the photons produced by synchrotron radiation. The other main model parameters are the electron temperature  $T_e$ , and the equipartition parameter between the magnetic field and the radiating (lepton) particle energy densities,  $k$ . A blackbody with temperature 4900 K, consistent with the companion star (Casares et al. 1993), is added to the model to account for the optical emission. An additional blackbody component has been also added to the fit, with normalization free to vary, in order to account for possible contribution from the outer disk. These photons are also included in the Comptonization. The ratio of the ‘nozzle’ (i.e. the pre-acceleration region) length to its radius has been fixed to 1.5, based on results in MNW05. The inclination angle between the jet axis and line of sight  $i$  has been fixed to  $43^\circ$ , the mass fixed to  $9.7 M_\odot$  and the distance to 1.2 kpc, according to the recent results by Froning et al. (2007). We wish to stress that adopting the system parameters inferred by Gelino et al. (2001) –i.e.  $11 M_\odot$  for the BH mass and  $i=40.75^\circ$ – does not result in a substantial change of the fitted parameters. Starting with parameter values similar to those found in other hard state BHBs, we have obtained a reasonable fit to the data, with  $\chi^2/\text{d.o.f.}=14.3/11$ . The best fit model is shown in Figure 4, with parameters and 90% confidence error bars given in Table 7.

## 5.2. Comparison to hard state sources

Most of the free parameters have landed in ranges which we are starting to recognize as ‘typical’ based on higher luminosity sources such as Cyg X-1 and GX 339-4 (MNW05), GRO J1655-40 (Migliari et al., submitted to ApJ) and the low luminosity AGN M81\* (Markoff et al., in prep.). Interestingly, the two main differences appear to be related to the acceleration and equipartition. In higher luminosity sources we have found ratios of magnetic energy density to the energy densities in radiating particles on the order of  $\sim 1 - 5$ ,

while here our best fit value actually favors a slight domination of the particle energy over the magnetic field ( $0.1 < k < 0.2$ ). The low error bar was limited by the value 0.1, and thus does not represent a complete exploration of the parameter space. Nevertheless, exact equipartition appears to be ruled out, pointing towards a change in energy distribution.

What is quite different compared to higher luminosity sources, however, is the required high-energy cutoff in the optically thin synchrotron component, and thus in the accelerated electron population. This is determined by the acceleration parameter  $f$  compared to the local cooling rates. We find  $f$  to be around two orders of magnitude lower for A0620–00 than in higher luminosity sources. Interestingly, the only other black hole we can study currently with similarly weak accretion is Sgr A\*, the Galactic Center super-massive BH. In fact, the jet model was first developed in simplified form by Falcke & Markoff (2000), with the aim to determine whether the same kind of model that could explain the inverted radio spectrum of Sgr A\* could also account for the newly discovered X-ray emission (Baganoff et al. 2000). They concluded that the SED of Sgr A\* does not require a power law of optically thin synchrotron emission after the break from its flat/inverted radio spectrum. Therefore, if the radiating particles have a power-law distribution, it must be so steep as to be indistinguishable from a Maxwellian in the optically thin regime, i.e. they must be only weakly accelerated<sup>3</sup>. Here we have shown that something similar, albeit less extreme, is occurring in the quiescent BHB A0620–00; either scenario implies that acceleration in the jets is absent or very inefficient at  $10^{-9} - 10^{-8}L_{\text{Edd}}$ .

## 6. Summary

We compile the radio/IR/optical spectra of three quiescent BHBs: V404 Cyg, XTE J1118+480 and A0620–00, for which we also present new optical SMARTS observations. Re-analysis of the archival *Spitzer* MIPS data for these systems yields systematically higher values for the statistical uncertainties related to sky subtraction with respect to the standard  $\sim 10\%$  value that is typically quoted for bright point-like sources. While our revised values for the 24  $\mu\text{m}$  fluxes are still consistent with those given by MM06 at the  $3\sigma$  level, they allow for a different interpretation of the measured mid-IR excess with respect to the tail of the donor star thermal component. We suggest that non-thermal emission from a jet could be responsible for a significant fraction (or all) of the measured excess mid-IR emission.

---

<sup>3</sup>In this framework, radically different particle distributions, such as power laws and Maxwellians, may result in similar fits as long as the characteristic particle energy (minimum and peak energy, respectively for the power law and the Maxwellian) is similar. See MNW05, Appendix.

While this possibly may not rule out the presence of circumbinary material, we argue that the radio/IR/optical spectra of the three BHBs under consideration do not require – in a statistical sense – the presence of an additional thermal component. A variability study could definitively address the question on the origin of the mid-IR excess, as, contrary to non-thermal jet emission, circumbinary disk emission is expected to be steady.

If non-thermal emission from a partially self-absorbed outflow is indeed responsible for the measured mid-IR excess, then the synchrotron luminosity of the jet, even excluding optically thin radiation from the base, exceeds the measured 2-10 keV luminosity by a factor of a few in all three systems. In turn, the jet mechanical power in quiescence is greater than the bolometric (0.1-100 keV) X-ray luminosity by several ( $\gtrsim 4$ ) orders of magnitude.

We proceed by focusing on A0620–00, the lowest Eddington-ratio BHB with a known radio counterpart, and construct its quiescent SED by adding VLA, *Spitzer*, SMARTS and *Chandra* data. In spite of the non-simultaneity of the *Spitzer* observations with the radio/optical/X-ray observations (which were taken over a two day period), we fit its broad-band SED of A0620-00 with a maximally jet-dominated model (MNW05). This is the first time that such a complex model is applied in the context of quiescent BHBs, and with the strong constraints on the jet break frequency cut-off provided by the *Spitzer* data in the mid-IR regime. In terms of best-fitting parameters, the major difference with respect to higher luminosity sources for which this model has been successfully tested is in the value of the acceleration parameter  $f$  compared to the local cooling rates, which turns out to be two orders of magnitude lower for A0620–00. This weak acceleration scenario is reminiscent of the Galactic Center super-massive BH Sgr A\*. Within the jet model working hypothesis, both SEDs are in fact consistent with the hard X-ray emission stemming primarily from inverse Compton processes in a corona/jet base which is dominated by quasi-thermal particles.

E.G. is funded by NASA through *Chandra* Postdoctoral Fellowship grant number PF5-60037, issued by the *Chandra* X-Ray Center, which is operated by the Smithsonian Astrophysical Observatory for NASA under contract NAS8-03060. J.A.T. acknowledges partial support from *Spitzer* contract number 1278068. C.D.B. is funded by NSF grant AST-0407063. S.B. acknowledges support by the Ing. Aldo Gini Foundation. We are grateful to Mike Nowak for providing us with the analysis scripts for ISIS.

## REFERENCES

Baganoff F. et al. 2000, Bulletin of the American Astronomical Society, 32, 1184



- Blandford R. & Begelman C., 1999, MNRAS, 303, L1
- Bradley C., Hynes R., Kong A., Haswell C., Casares J., Gallo E., 2007, ApJ, in press (arXiv:astro-ph/07062652v1)
- Cardelli J., Clayton, G., Mathis, J., 1989, ApJ, 345, 245
- Casares J., Charles P. A., Naylor T., Pavlekno E. P., 1993, MNRAS, 265, 834
- Corbel S., Tomsick J., Kaaret P., 2006, ApJ, 636,
- Corbel S., Nowak M., Fender R. P., Tzioumis A. K., Markoff S., 2003, A&A, 400, 1007
- Corbel S. & Fender R., 2002, ApJ, 573, L35
- Dale D. et al. 2005, ApJ, 633, 857
- Falcke H. & Markoff S., 2000, A&A, 362, 113
- Falcke H. & Biermann P. L., 1996, A&A, 308, 321
- Fazio G. et al. 2004, ApJS, 154, 10
- Fender R. P., 2006, in Lewin W. H. G., van der Klis M., eds, Compact Stellar X-Ray Sources. Cambridge Univ. Press, Cambridge
- Fender R. P., Belloni T., Gallo E., 2004, MNRAS, 355, 1105
- Fender R. P., Gallo E., Jonker P. G., 2003, MNRAS, 343, L99
- Fender R. P., 2001, MNRAS, 322, 31
- Froning C., Robinson E., Bitner M., 2007, ApJ, in press (arXiv:astro-ph/07040267v1)
- Gallo E., 2007, in Proc. of ‘The Multicolored Landscape of Compact Objects and their Explosive Origins’, AIP Conf. Proc. (arXiv:astro-ph/0702126v1)
- Gallo E. et al. 2006, MNRAS, 370, 1351
- Gallo E., Fender R. P., Hynes R. I., 2005b, MNRAS, 356, 1017
- Gallo E., Fender R., Kaiser, C., Russell, D., Morganti, R., Oosterloo, T., Heinz, S., 2005a, Nature, 436, 819
- Gallo E., Fender R. P., Pooley G. G., 2003, MNRAS, 344, 60

- Gelino D., Balman S., Kiziloglu Ü., Yilmaz A., Kalemci E., Tomsick J., 2006, *ApJ*, 642, 438
- Gelino D. M., Harrison T. E., Orosz J. E. 2001, *AJ*, 122, 2668
- Heinz S. & Sunyaev R., 2003, *MNRAS*, 343, L59
- Heinz S. & Grimm H.-J. 2005, *ApJ*, 633, 384
- Hjellming P. M., Rupen M. P., Mioduszewski A. J., Narayan R., 2000, *ATel* 54
- Homan J., Buxton, M., Markoff, S., Bailyn, C., Nespoli, E., Belloni, T., 2005, *ApJ*, 624, 295
- Homan J. & Belloni T., 2005, *A&SS*, 300, 107
- Houck J. & De Nicola L., 2000, in *ASP Conf. Ser.*, Vol. 216, *Astronomical Data Analysis Software and Systems IX*, eds. N. Manset, C. Veillet, D. Crabtree (San Francisco: ASP), 591
- Hynes R. et al. 2006, *ApJ*, 651, 401
- Hynes R. et al. 2004, *ApJ*, 611, L125
- Hynes R. I. et al. 2003, *MNRAS*, 345, 292
- Körding E., Fender R., Migliari S., 2006, *MNRAS*, 369, 1451
- Makovoz D. & Marleau F., 2005, *PASP*, 117, 1113
- Markoff S., Nowak M. A., Wilms J., 2005, *ApJ*, 635, 1203 (MNW05)
- Markoff S. & Nowak M. A., 2004, *ApJ*, 609, 972
- Markoff S., Nowak, M., Corbel, S., Fender, R., Falcke, H., 2003, *A&A*, 397, 645
- Markoff S., Falcke H., Fender R., 2001, *A&A*, 372, L25
- Miller J., Homan, J., Steeghs, D., Rupen, M., Hunstead, R. W., Wijnands, R., Charles, P. A., Fabian, A. C., 2006a, *ApJ*, 653, 525
- Miller J., Homan, J., Miniutti G., 2006b, *ApJ*, 652, L113
- McClintock J. E., Remillard R. A., 2006, in Lewin W. H. G., van der Klis M., eds, *Compact Stellar X-Ray Sources*. Cambridge Univ. Press, Cambridge
- McClintock J. E. et al. 2003, *ApJ*, 593, 435

- Migliari S., Tomsick, J., Maccarone, T., Gallo, E., Fender, R., Nelemans, G., Russell, D., 2006, *ApJ*, 643, L41
- Mirabel I. F., Dhawan V., Mignani R., Rodrigues I., Giglielmetti F., 2001, *Nature*, 413, 139
- Muno M. & Mauerhan J., 2006, *ApJ*, 648, L135 (MM06)
- Nowak, M.; Wilms, J., Heinz, S., Pooley, G., Pottschmidt, K., Corbel, S., 2005, *ApJ*, 629, 1006
- Narayan R., Yi I. 1994, *ApJ*, 428, L13
- Rieke G. et al. 2004, *ApJS*, 154, 25
- Russell D., Fender R., Gallo E., Kaiser C., 2007, *MNRAS*, 376, 1341
- Russell, D., Fender, R., Hynes, R., Brocksopp, C., Homan, J., Jonker, P., Buxton, M., 2006, *MNRAS*, 371, 1334 (R06)
- Rykoff E., Miller J., Steeghs D., Torres M., 2007, submitted to *ApJ* (arXiv:astro-ph/0703497v1)
- Shahbaz T., Dhillon V. S., Marsh T. R., Zurita C., Haswell C. A., Charles P. A., Hynes R. I., Casares J., 2003, *MNRAS*, 346, 1116
- Taam R. & Spruit H., 2001, *ApJ*, 561, 329
- Wang Z., Chakrabarty D., Kaplan D., 2006, *Nature*, 440, 772
- Wu C.-C., Aalders J., van Duinen R., Kester D., Wesselius P., 1976, *A&A*, 50, 445
- Xue Y. & Cui W., 2007, *A&A*, 466, 1053
- Yuan F., Cui W., Narayan R., 2005, *ApJ*, 620, 905
- Zurita C., Casares J., Hynes R., Shahbaz T., Charles P., Pavlenko E., 2004, *MNRAS*, 352, 877
- Zurita C., Casares J., Shahbaz T., 2003, *ApJ*, 582, 369

Table 1. Spitzer observations of quiescent black hole binaries.

Target	Method	Flux ( $\mu\text{Jy}$ )		
		4.5 $\mu\text{m}$	8.0 $\mu\text{m}$	24.0 $\mu\text{m}$
V404 Cyg	Ap. Photometry	3336	1820	414 $\pm$ 220
	PRF fitting	3220	1760	436 $\pm$ 220
XTE J1118+480	Ap. Photometry	69	59	<50
	PRF fitting	69	58	<50
A0620-00	Ap. Photometry	412	288	138 $\pm$ 65
	PRF fitting	380	305	121 $\pm$ 65

Note. — Un-dereddened values. Unless otherwise noted, flux errors are taken to be 10%, due to calibration systematic errors. For the extinction corrections, we used the following values: V404 Cyg:  $A_V=2.8$  (Shahbaz et al. 2003); XTE J1118+480:  $A_V=0.06$  (Gelino et al. 2006); A0620-00:  $A_V=1.2$  (Wu et al. 1983).

Table 2. Single blackbody fits to the IR-optical spectra

Target (1)	$R/D$ (2)	$T_{\text{fit}}$ (3)	$T_{\text{star}}$ (4)	$\chi^2/\text{d.o.f.}$ (5)
V404 Cyg	$5.4 \pm 0.2$	$4533 \pm 80$	5500	10.3/7
XTE J1118+480	$0.7 \pm 0.1$	$3850 \pm 113$	4250	69.6/5
A0620-00	$2.0 \pm 0.1$	$4468 \pm 104$	4900	21.8/4

Note. — Columns are: (1) Source name; (2) Fitted star radius over distance,  $R/D$ , times  $10^{-11}$ ; (3) Fitted star temperature,  $T_{\text{fit}}$ , in  $K$ ; (4) Star temperatures as found in the literature,  $T_{\text{star}}$ , in  $K$  (references for the star temperature and system inclination and distance are the same as listed in the caption of Table 1 for the extinction values); (5) Fitted  $\chi^2$  over degrees of freedom (d.o.f.).

Table 3. Double blackbody fits to the IR-optical spectra

Target (1)	$(R/D)_1$ (2)	$T_{\text{fit},1}$ (3)	$(R/D)_2$ (4)	$T_{\text{fit},2}$ (5)	$\chi^2/\text{d.o.f.}$ (6)
V404 Cyg	$5.09 \pm 0.02$	$4623 \pm 94$	$30 \pm 18$	$489 \pm 169$	1.4/5
XTE J1118+480	$0.55 \pm 0.04$	$4234 \pm 150$	$4 \pm 1$	$754 \pm 140$	12.0/3
A0620-00	$1.7 \pm 0.1$	$4691 \pm 149$	$23 \pm 10$	$393 \pm 83$	2.0/2

Note. — Columns are: (1) Source name; (2)&(4) Fitted blackbody radius over distance, times  $10^{-11}$ ; (3)&(5) Fitted blackbody temperature, in  $K$ ; (6) Reduced  $\chi^2$ . Subscripts 1 and 2 indicate the first and second blackbody components.

Table 4. Blackbody + broken power law fits to the radio-IR-optical spectra.

Target (1)	$(R/D)$ (2)	$T_{\text{fit}}$ (3)	$F_{\nu_0}$ (4)	$\alpha_1$ (5)	$\chi^2/\text{d.o.f.}$ (6)
V404 Cyg	$5.0 \pm 0.2$	$4626 \pm 94$	$448 \pm 189$	$0.02 \pm 0.04$	4.0/9
XTE J1118+480	$0.5 \pm 0.1$	$4302 \pm 211$	$62 \pm 23$	$0.27 \pm 0.39$	6.2/3
A0620-00	$1.54 \pm 0.03$	$4897 \pm 6$	$148 \pm 1$	$0.113 \pm 0.001$	7.8/3

Note. — Columns are: (1), (2), (3): see Table 1; (4) Fitted power law normalization at  $\nu_0 = 10^{14}$  Hz, in  $\mu\text{Jy}$  (the broken power-law expression is given in equation 1; we fixed  $\nu_b = 10^{14}$  Hz and  $\alpha_2 = -0.8$ ); (5) Fitted power law index below  $\nu_b$ ; (6) Reduced  $\chi^2$ .

Table 5. A0620–00: SMARTS observations

Band	UT start	mag <sup>a</sup>	Flux <sup>b</sup> ( $\mu$ Jy)
<i>V</i>	05Aug18-09:28:15	17.75 $\pm$ 0.03	884 $\pm$ 68
<i>I</i>	05Aug18-09:19:31	16.04 $\pm$ 0.05	1673 $\pm$ 161
<i>H</i>	05Aug18-09:28:12	14.6 $\pm$ 0.1	1910 $\pm$ 283

Note. — <sup>a</sup>Un-reddened values.

<sup>b</sup>De-reddened values (adopting  $A_V=1.2$ ), allowing for an extra 0.05 mag uncertainty due to systematic calibration errors.



Table 6. Jet power

Target (1)	$\alpha_1$ (2)	D (3)	$L_{j,\text{tot}}$ (4)	$L_{j,\text{rad}}/L_X$ (5)
V404 Cyg	0.022	4	$>1.7 \times 10^{34}$	2.8
XTE J1118+480	0.270	1.8	$>3.7 \times 10^{32}$	5.4
A0620-00	0.113	1.2	$>4.5 \times 10^{32}$	3.8

Note. — Columns are: (1) Source name; (2) Fitted jet spectral index below  $\nu_b = 10^{14}$  Hz; (3) Distance, in kpc; (4) *Total* (kinetic + radiative) jet power, in  $\text{erg s}^{-1}$ ; (5) Ratio between the *radiative* jet power, integrated up to  $\nu_b$ , and the quiescent X-ray luminosity  $L_X$ , between 2–10 keV.  $L_{j,\text{tot}}$  is calculated assuming no Doppler boosting, and a (conservative) 5% radiative efficiency; as such, it represents a strict lower limit to the total jet power. Accordingly,  $L_{j,\text{rad}} = 0.05 \times L_{j,\text{tot}}$  only accounts for the partially self-absorbed synchrotron emission from the jet. Quiescent X-ray luminosities are taken from: V404 Cyg: Garcia et al. (2001), Kong et al. (2002), Hynes et al. (2004). XTE J1118+480: McClintock et al. (2004). A0620-00: Kong et al. (2002), Gallo et al. (2006).

Table 7. Jet Model for A0620–00

$N_{\text{H}}$ (1)	$N_{\text{j}}$ (2)	$r_0$ (3)	$z_{\text{acc}}$ (4)	$T_{\text{e}}$ (5)	$p$ (6)	$f$ (7)	$k$ (8)	$BB_{\text{norm}}$ (9)
$3.6^{+0.7}_{-1.1}$	$14.6^{+0.4}_{-7.3}$	$3.9^{+2.2}_{-0.1}$	$25^{+272}_{-2}$	$2.57^{+0.29}_{-0.01}$	$2.5^{+0.1}_{-0.3}$	$5.1^{+1.0}_{-1.5}$	$0.1^{+0.1}_{-0.0}$	$0.5^{+0.2}_{-0.1}$

Note. — Columns are: fitted (1) Hydrogen equivalent column density, in  $10^{22} \text{ cm}^{-2}$ ; (2) Model internal normalization, expressed in units of  $10^{-4} L_{\text{Edd}}$ : it dictates the power divided by the particles and the magnetic field at the base; (3) Jet base (or ‘nozzle’) radius, in units of gravitational radii  $r_g = GM_{\text{BH}}/c^2$ ; (4) Acceleration region,  $z_{\text{acc}}$ , in  $r_g$ ; it sets the location along the jet at which (a fraction of) the particles start being accelerated; (5) Temperature of the relativistic quasi-Maxwellian distribution with which the leptons enter the jet, in  $10^{10} \text{ K}$ ; (6) Power law index of the accelerated electron distribution,  $p$ , where  $N(E) \propto E^{-p}$ ; (7) Acceleration parameter,  $f$ , in units of  $10^{-6}$ : sets the balance between particle acceleration and radiative plus adiabatic cooling, such that the quasi-thermal particles be energized into a power-law tail; (8) Equipartition parameter,  $k = (u_{\text{B}}/u_{\text{rad}})$ : the ratio between the energy density in radiating leptons and the magnetic field energy density; (9) Internal disk blackbody normalization, in  $10^{30} \text{ erg s}^{-1}$ . We fixed the BH mass, distance and inclination of A0620–00 to:  $9.7 M_{\odot}$ , 1.2 kpc and  $43^{\circ}$  (Froning et al. 2007), yielding  $\chi_{\text{red}}^2 = 1.3$ . Similar parameters, within the errors, are obtained adopting a mass of  $11 M_{\odot}$  and inclination of  $40.75^{\circ}$  (Gelino et al. 2001). Error bars are given at the 90% confidence level.

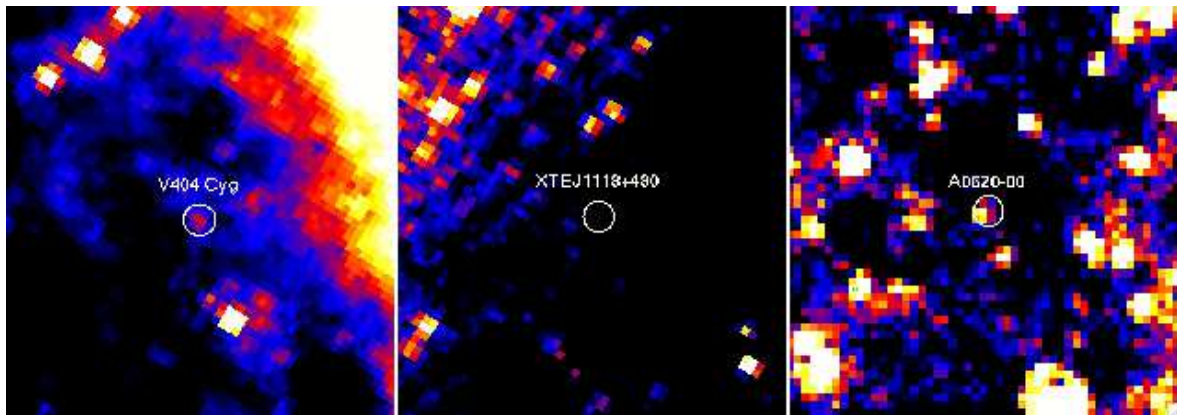


Fig. 1.— *Spitzer* MIPS 24  $\mu\text{m}$  images of V404 Cyg, XTE J1118+480, and A0620–00. White circles (with 2 arcsec radius) mark the position of the radio counterparts, from MERLIN and VLA observations for V404 Cyg (R. Spencer and M. Rupen, private communications); VLA for A0620–00 (Gallo et al. 2006); MERLIN for XTE J1118+480 (Fender et al. 2001). The fields of view of V404 Cyg and A0620–00 are evidently affected by high background contaminations, resulting in high statistical uncertainties related to sky subtraction. For reference, 1 MIPS pixel corresponds to 1.2 arcsec in size. North is at the top, and East is to the left of these images.

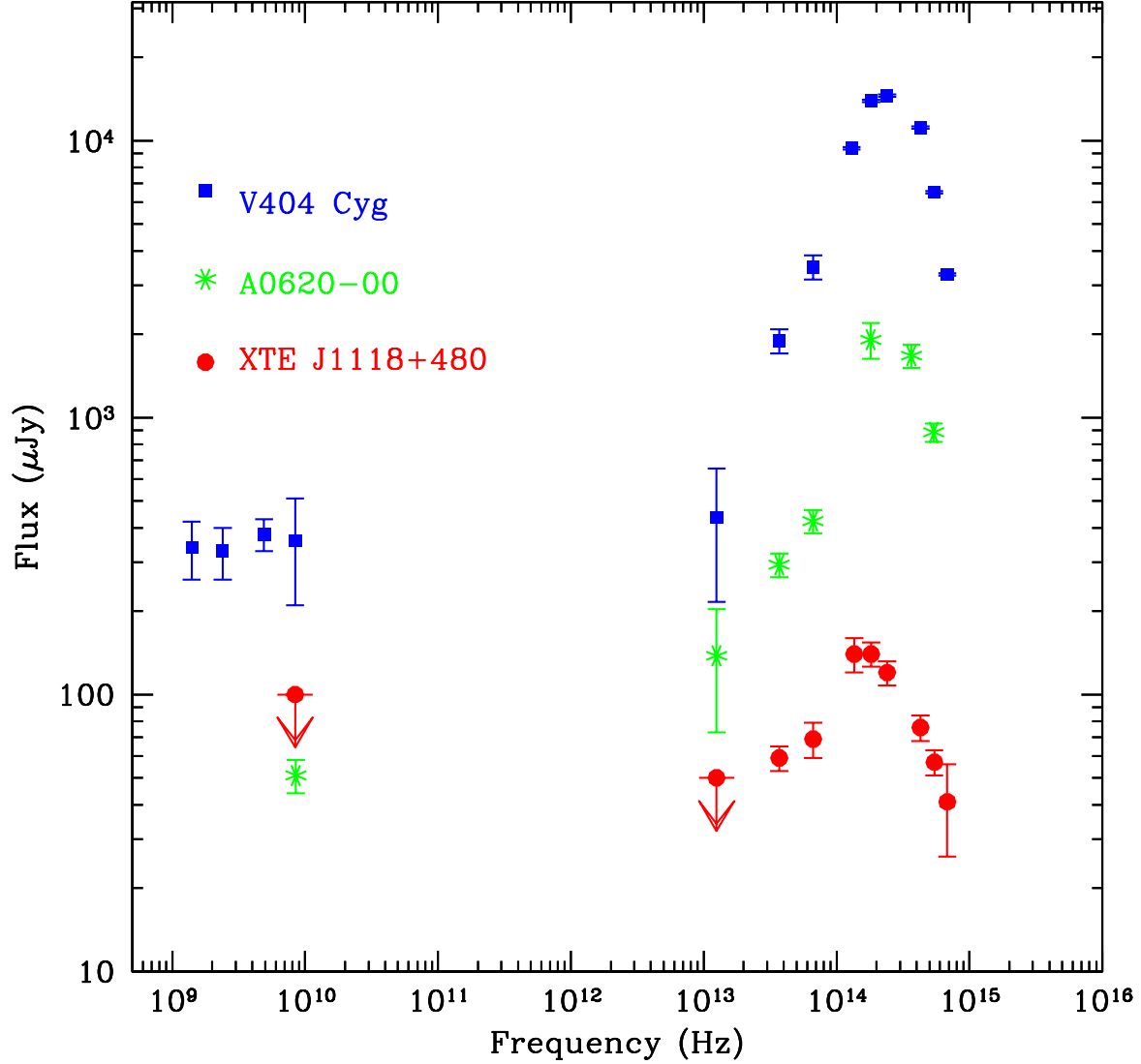


Fig. 2.— Composite radio/IR/optical spectra of quiescent black hole binaries. *V404 Cyg*: radio data from Gallo et al. (2005b), taken in 2002; IR data from this work, taken in 2004-2005; optical photometry from Casares et al. 1993, taken between 1990-1992. *A0620-00*: radio data from Gallo et al. (2006), acquired in August 2005; IR and optical data from this work. The data span a period of 5 months, with nearly simultaneous radio/optical coverage. *XTE J1118+480*: radio upper limit from Mirabel et al. (2001); IR data from this work; optical photometry from Gelino et al. (2006).

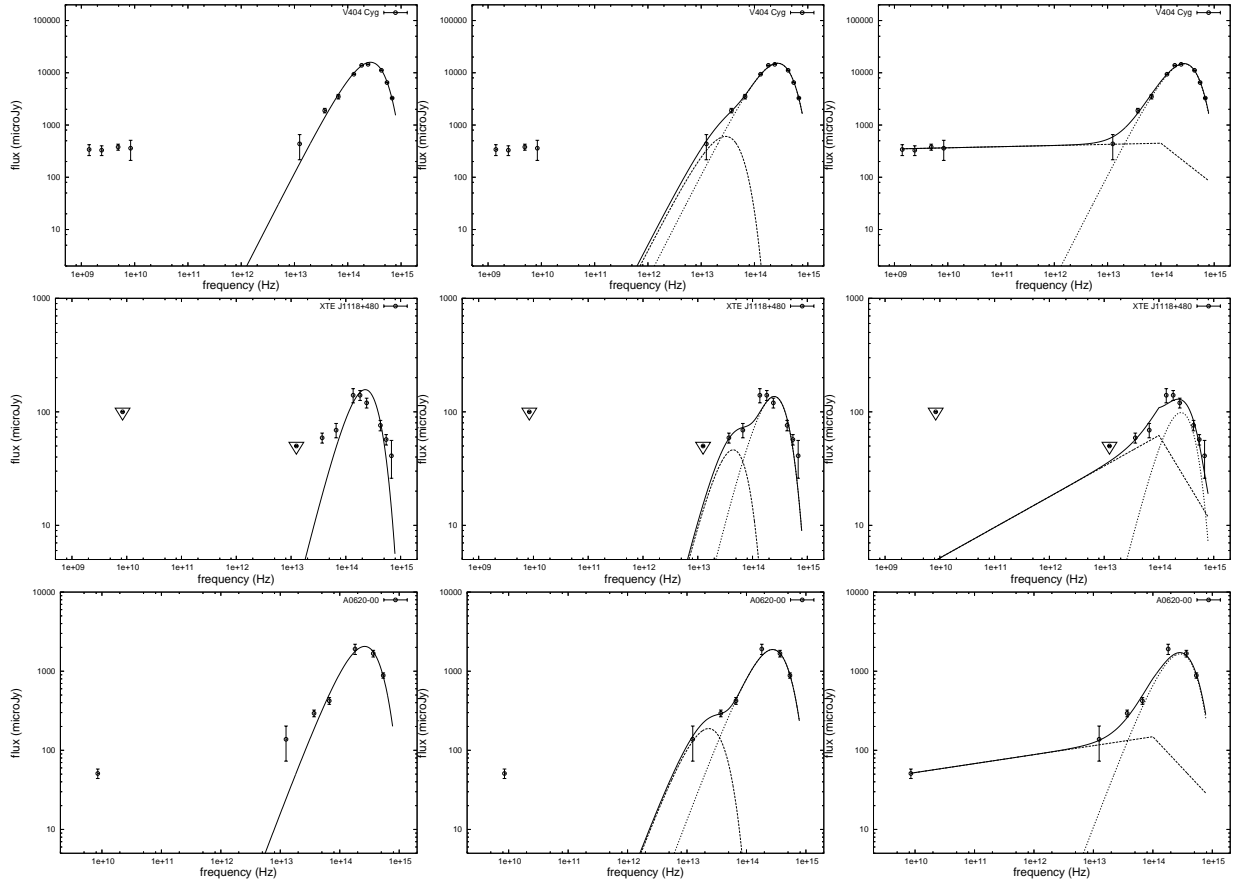


Fig. 3.— From top to bottom: V404 Cyg, XTE J1118+480, A0620-00. Curves on the left panels show the fits to the IR/optical data with a single blackbody curve (see Table 2 for the fitted parameters); curves in middle are for a double blackbody fit (Table 3); the right panels show the fit to the radio-IR-optical SEDs with a single blackbody plus a broken power law (Table 4).

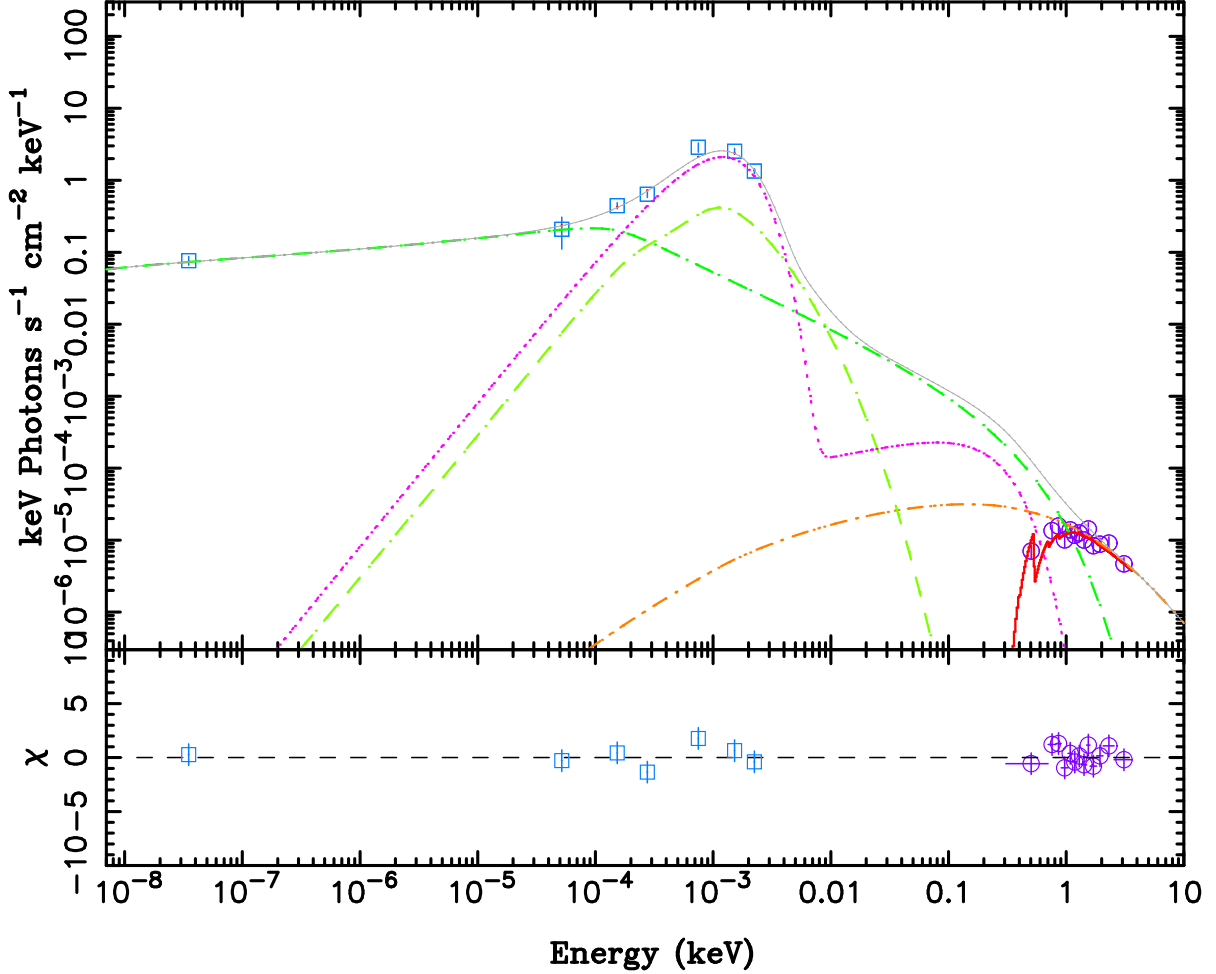


Fig. 4.— Jet model fit to broadband A0620-00 data with residuals. The symbols represent the data, while the solid red line is the model fit in detector space. Other indicated components are not convolved with the detector matrices nor do they include absorption, and serve only to illustrate how the various emission mechanisms and regions contribute to the continuum. Solid (gray): total spectrum; Dot-long-dashed (light green): pre-acceleration inner jet synchrotron emission; Dot-long-dashed (darker green): post-acceleration outer jet synchrotron; Dot-dash-dash (orange): Compton emission from the inner jet, including external disk photons as well as synchrotron self-Compton; Dot-short-dash (magenta): thermal multicolor-blackbody disk model plus single blackbody representing the star. See Table 7 for the fitted parameters.